

Ultra-low thermal expansion realized in giant negative thermal expansion materials through self-compensation

Fei-Ran Shen, Hao Kuang, Feng-Xia Hu, Hui Wu, Qing-Zhen Huang, Fei-Xiang Liang, Kai-Ming Qiao, Jia Li, Jing Wang, Yao Liu, Lei Zhang, Min He, Ying Zhang, Wen-Liang Zuo, Ji-Rong Sun, and Bao-Gen Shen

Citation: *APL Materials* **5**, 106102 (2017);

View online: <https://doi.org/10.1063/1.4990481>

View Table of Contents: <http://aip.scitation.org/toc/apm/5/10>

Published by the [American Institute of Physics](#)

Articles you may be interested in

[Reduction of in-plane field required for spin-orbit torque magnetization reversal by insertion of Au spacer in Pt/Au/Co/Ni/Co/Ta](#)

APL Materials **5**, 106104 (2017); 10.1063/1.4991950

[Accurate quantification of glass-forming ability by measuring effective volume relaxation of supercooled melt](#)

APL Materials **5**, 106103 (2017); 10.1063/1.4999357

[Aperiodic-metamaterial-based absorber](#)

APL Materials **5**, 096107 (2017); 10.1063/1.4996112

[Theoretical prediction of fracture conditions for delithiation in silicon anode of lithium ion battery](#)

APL Materials **5**, 106101 (2017); 10.1063/1.4997978

[Electrostatically tuned dimensional crossover in LaAlO₃/SrTiO₃ heterostructures](#)

APL Materials **5**, 106107 (2017); 10.1063/1.4999804

[Fish-inspired self-powered microelectromechanical flow sensor with biomimetic hydrogel cupula](#)

APL Materials **5**, 104902 (2017); 10.1063/1.5009128



**FIND THE NEEDLE IN THE
HIRING HAYSTACK**

POST JOBS AND REACH THOUSANDS OF
QUALIFIED SCIENTISTS EACH MONTH.

PHYSICS TODAY | JOBS
WWW.PHYSICSTODAY.ORG/JOBS

Ultra-low thermal expansion realized in giant negative thermal expansion materials through self-compensation

Fei-Ran Shen,^{1,2} Hao Kuang,^{1,2} Feng-Xia Hu,^{1,2,a} Hui Wu,³
 Qing-Zhen Huang,⁴ Fei-Xiang Liang,^{1,2} Kai-Ming Qiao,^{1,2} Jia Li,^{1,2}
 Jing Wang,^{1,2,a} Yao Liu,^{1,2} Lei Zhang,⁵ Min He,^{1,2} Ying Zhang,^{1,2}
 Wen-Liang Zuo,^{1,2} Ji-Rong Sun,^{1,2} and Bao-Gen Shen^{1,2}

¹Beijing National Laboratory for Condensed Matter Physics and State Key Laboratory of Magnetism, Institute of Physics, Chinese Academy of Sciences, Beijing 100190, People's Republic of China

²School of Physical Sciences, University of Chinese Academy of Sciences, Beijing 100049, People's Republic of China

³Department of Materials Science and Engineering, University of Maryland, College Park, Maryland 20742-2115, USA

⁴NIST Center for Neutron Research, National Institute of Standards and Technology, Gaithersburg, Maryland 20899, USA

⁵High Magnetic Field Laboratory, Chinese Academy of Sciences, Hefei 230031, People's Republic of China

(Received 15 June 2017; accepted 20 September 2017; published online 11 October 2017)

Materials with zero thermal expansion (ZTE) or precisely tailored thermal expansion are in urgent demand of modern industries. However, the overwhelming majority of materials show positive thermal expansion. To develop ZTE or negative thermal expansion (NTE) materials as compensators has become an important challenge. Here, we present the evidence for the realization of ultra-low thermal expansion in Mn–Co–Ge–In particles. The bulk with the Ni₂In-type hexagonal structure undergoes giant NTE owing to a martensitic magnetostructural transition. The major finding is that the thermal expansion behavior can be totally controlled by modulating the crystallinity degree and phase transition from atomic scale. Self-compensation effect leads to ultra-low thermal expansion with a linear expansion coefficient as small as $+0.68 \times 10^{-6}/\text{K}$ over a wide temperature range around room temperature. The present study opens an avenue to reach ZTE particularly from the large class of giant NTE materials based on phase transition. © 2017 Author(s). All article content, except where otherwise noted, is licensed under a Creative Commons Attribution (CC BY) license (<http://creativecommons.org/licenses/by/4.0/>). <https://doi.org/10.1063/1.4990481>

Materials with ultra-low thermal expansion or zero thermal expansion (ZTE) are being widely used in manufacturing industry,^{1–3} such as precision engineered parts, optical mirrors, and printed circuit boards. ZTE is generally realized through combining positive thermal expansion (PTE) and negative thermal expansion (NTE) materials. The ultra-low thermal expansion in the widely used glass ceramics is based on the combined effect of NTE from complex main crystalline phases and PTE from the glass matrix.^{4,5} To meet various applications, many efforts have been dedicated to search for NTE materials because compared with the vast number of PTE materials there are only a few compounds that were discovered showing NTE, e.g., ZrW₂O₈ (Ref. 6), CuO nanoparticles,⁷ PbTiO₃-based compounds,⁸ (Bi,La)NiO₃ (Ref. 9), antiperovskite manganese nitrides,^{10–13} La(Fe,Co,Si)₁₃ (Ref. 14), MnCoGe-based materials,¹⁵ and reduced Ca₂RuO₄ (Ref. 16). Among these NTE materials, the phase-transition-type materials^{10–15} have attracted particular attention, which utilize the large volume contraction on heating during phase transition. Besides ZTE composites, several pure compounds have been discovered showing ZTE, such as CuO micrometer-sized particles,³ YbGaGe (Ref. 17), Mn₃AN (A = Cu/Sn, Zn/Sn) (Ref. 18), N(CH₃)₄CuZn(CN)₄

^aElectronic addresses: fxhu@iphy.ac.cn and wangjing@iphy.ac.cn

(Ref. 19), and Fe[Co(CN)₆] (Ref. 20). Although several materials have been identified as useful ZTE or NTE materials, novel approaching to ultra-low thermal expansion still remains as a high challenge.

Hexagonal MM'X (M and M': transition element, X: main group element) compounds exhibit rich magnetic and structural properties.^{21–24} The ground state can be ferromagnetic or antiferromagnetic depending on the specific atomic local environments and exchange coupling. As a family member, MnCoGe-based compounds undergo a martensitic structural transition from the Ni₂In-type hexagonal (space group P63/mmc) to TiNiSi-type orthorhombic (space group Pnma) structure with a negative expansion of unit cell volume as large as $\Delta V/V \sim 3.9\%$. The optimized compositions with concurrent magnetic and structural transitions have been discovered showing large magnetocaloric and barocaloric effect.^{22–24} Moreover, as NTE materials, giant NTE in a very wide temperature window has been realized in the bonded MnCoGe-based compounds.¹⁵ The achieved average linear thermal expansion coefficient, $\bar{\alpha}$, can be as much as $-51.5 \times 10^{-6}/\text{K}$ in a temperature window as wide as 210 K from 122 to 332 K in a bonded compound, which originates from the lattice expansion in a broadened martensitic structural transformation with assistance of residual stress. Here, we choose the giant NTE material and report the realization of ultra-low thermal expansion by controlling the crystallinity degree and phase transition. The polycrystalline MnCoGe_{0.99}In_{0.01} alloy undergoes a concurrent magnetic and structural transition around $T_{\text{mstru}} \sim 315$ K.¹⁵ Our investigations demonstrated that a large amount of sample can be converted into an amorphous structure through energetic ball milling. This part turns to show PTE, while the remained crystallites show reduced NTE in a significantly broadened temperature window due to the instability of martensitic magnetostructural transformation caused by residual stress and atomic defects. Hence, self-compensation effect leads to ultra-low thermal expansion and totally adjustable NTE by controlling crystallinity degree.

Mn–Co–Ge–In particles were prepared through energetic ball milling in the protection of Ar atmosphere from MnCoGe_{0.99}In_{0.01} alloys, which were fabricated by conventional arc-melting technique.²⁴ The particle size was controlled by milling time. Five samples with different particle sizes were made, namely, P1 (10–20 μm), P2 (5–10 μm), P3 (2–5 μm), P4 (1–2 μm), and P5 (0.3–1 μm). For the small particles P4 (1–2 μm) and P5 (0.3–1 μm), high-resolution transmission electron microscopy (TEM) images manifest the mixture of a large amount of amorphous structures that lost long-range atomic order and nanocrystallites full of atomic defects [circled regions in Figs. 1(a) and 1(b)]. The average crystallite sizes are about 15 nm and 8 nm for P4 (1–2 μm) and P5 (0.3–1 μm), respectively. The amounts of the amorphous structure estimated from high-resolution neutron powder diffraction (NPD) are about 20%, 30%, and 40%, for P3 (2–5 μm), P4 (1–2 μm), and P5 (0.3–1 μm), respectively (details can be found in the [supplementary material](#)). Clearly, the amorphous-like structure increases and the crystallite size reduces with extended milling time. The appearance of the dispersed Debye ring in the electron diffraction pattern [lower left quarter of Figs. 1(a) and 1(b)] further evidences the coexistence of crystallites with the structure that lost long-range atomic order. For comparison, the results for big particles P1 (10–20 μm) are given in Fig. S1 (TEM/SEM results in Fig. S1 of the [supplementary material](#)).

We measured linear expansion $\Delta L/L$ using high-resolution strain gauge for the bonded particles (details of sample preparation can be found in the [supplementary material](#)). Figure 2 shows $\Delta L/L$ with respect to temperature for the representative particles in comparison with the bulk. The maximal $\Delta L/L$ amounts to -1.02×10^{-2} from 192 K to 310 K ($\Delta T \sim 108$ K) for the bulk,¹⁵ but it declines with the reduced particle size and crystallinity degree while the operating ΔT significantly broadens. For P1 (10–20 μm), the maximal $\Delta L/L$ reduces to -6076×10^{-6} , while the ΔT extends to 154 K (156–310 K). With further reducing the particle size and crystallinity degree, the maximal $\Delta L/L$ further reduces and the operating ΔT further extends. For P3 (2–5 μm) and P4 (1–2 μm), NTE prevails in the entire temperature range from 310 K down to 100 K. Correspondingly, the evaluated average linear NTE coefficients, $\bar{\alpha}$, are $-94.7 \times 10^{-6}/\text{K}$ (192–310 K), $-39.5 \times 10^{-6}/\text{K}$ (156–310 K), $-14.1 \times 10^{-6}/\text{K}$ (100–310 K), and $-3.9 \times 10^{-6}/\text{K}$ (100–290 K), for the bulk P1 (10–20 μm), P3 (2–5 μm), and P4 (1–2 μm), respectively.

More attractively, for the smallest particles P5 (0.3–1 μm), the negative NTE behavior disappears and turns to be ultra-low positive PTE with α coefficient as small as $\sim +0.68 \times 10^{-6}/\text{K}$

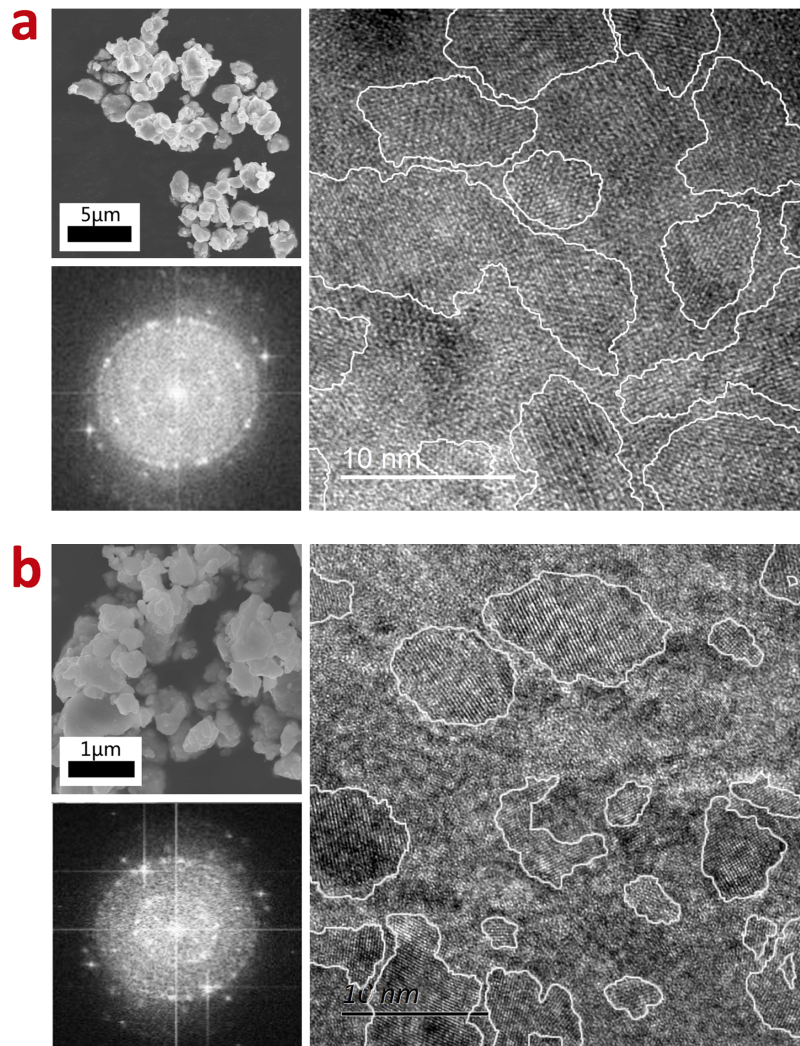


FIG. 1. SEM image, high-resolution TEM image, and electron diffraction pattern from Fourier transform. (a) P4 (1–2 μm) and (b) P5 (0.3–1 μm), circled regions by the white line indicate the nanocrystallites.

from 200 K to 310 K. Such a largely tunable thermal expansion behavior suggests that the material can be greatly useful as a direct ZTE material, in addition to be as compensators for PTE material. Here, it is noteworthy that the low NTE in P4 (1–2 μm) and the ultra-low PTE in P5 (0.3–1 μm) remain nearly independent of temperature in the corresponding temperature window, which is guided by the pink lines in Fig. 2. These characteristics are appreciable for practical application.

Such tunable thermal expansion with particle size should come from the combined effect from the crystalline phases and the coexistent amorphous structure, particularly for the small particles. To examine the contribution from the overall crystallites, variable temperature x ray diffraction (XRD) and neutron powder diffraction (NPD) experiments were performed for the various particles before bonding (details can be found in the [supplementary material](#)). Careful refinements indicated that the phase ratio changes remarkably with crystallite size, as shown in Fig. 3. A large amount of austenitic phases loses the martensitic structural transition and keeps the hexagonal structure down to low temperature in the small crystallites. The ratio of the hexagonal structure is about 7%, 14.5%, 38.5%, 44.8%, and 55.2% at a low temperature of 35 K, far away from the martensitic magnetostructural transformation $T_{\text{mstru}} \sim 315$ K,¹⁵ indicating that at least the same ratio of austenitic phase lost the martensitic transformation for the particles P1 (10–20 μm), P2 (5–10 μm), P3 (2–5 μm), P4 (1–2 μm),

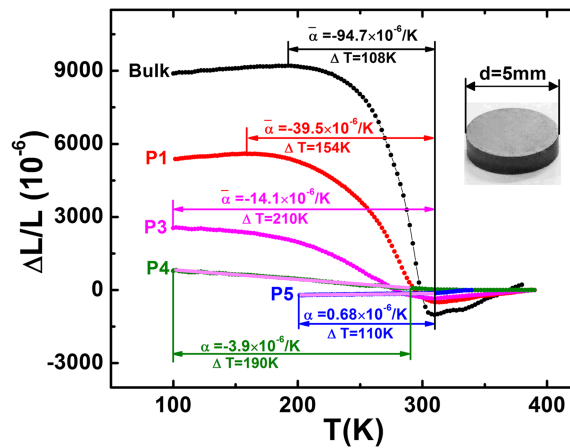


FIG. 2. Linear thermal expansion $\Delta L/L$ for the bonded particles compared with the bulk (the reference temperature is 390 K). Particle size: P1 (10–20 μm), P3 (2–5 μm), P4 (1–2 μm), and P5 (0.3–1 μm). The inset shows the morphology of the bonded particles. The low NTE in P4 (1–2 μm) and the ultra-low PTE in P5 (0.3–1 μm) remain nearly independent of temperature in the corresponding temperature window, which is guided by the pink lines. The $\Delta L/L$ -T curve of the bulk is cited from Ref. 15.

and P5 (0.3–1 μm), respectively. Meanwhile, the remained martensitic structural transition gradually broadens with reducing the crystallite size. Magnetic measurements also verified the instability of martensitic magnetostructural transformation with varying crystallite size (details can be found in Fig. S2 of the [supplementary material](#)). Such instability of the martensitic transformation will lead to a reduced NTE.

A unique feature of the hexagonal Mn–Co–Ge–In materials is the high sensitivity of martensitic magnetostructural transformation to stress.^{23–25} An introduced stress can impact the martensitic magnetostructural transformation through altering the atomic local environments, strength of covalent bonding, and the width of effective 3d bands, and hence a giant barocaloric effect has been observed.²⁴ For the small particles, the appearance of the amorphous structure as grain boundaries can be understandable considering the significant impact of high-energy ball milling on the structure. A simulation on the deformation of nanocrystalline grains revealed that lattice will be softened due to a large fraction of disordered atoms (30%-50%) at grain boundaries.²⁶ Moreover, a study on the strained nanoparticles²⁷ indicated that lattice compression and possible disorder inside nanocrystalline grains

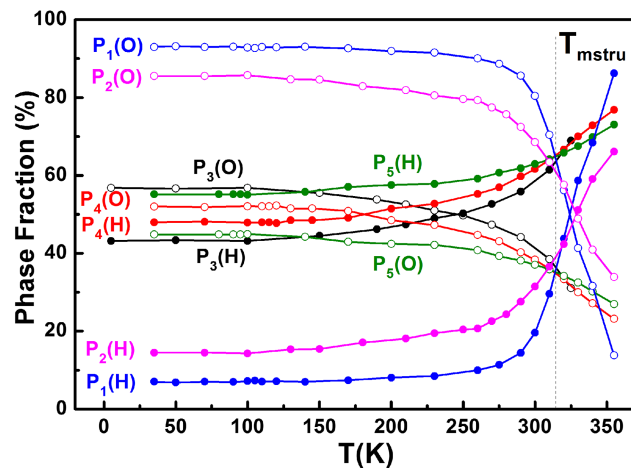


FIG. 3. Phase fraction as a function of temperature for various particles, P1 (10–20 μm), P2 (5–10 μm), P3 (2–5 μm), P4 (1–2 μm), and P5 (0.3–1 μm). At low temperatures, a high ratio of the hexagonal (H) structure appears and coexists with the orthorhombic (O) structure, particularly for small particles P3 (2–5 μm), P4 (1–2 μm), and P5 (0.3–1 μm) indicating that at least the same ratio of austenitic phase loses the martensitic transformation for the overall crystallines. Meanwhile, the remained martensitic structural transition gradually becomes broadening with the reduced crystalline size.

can largely affect electronic properties and make the nanoparticles exhibit distinct material properties from their bulk. Our refinements based on XRD and NPD, as well as selected-area electron diffraction, revealed the contraction of a unit cell with reducing grain size (Table S1 and Fig. S3 of the [supplementary material](#)). Meanwhile, many defects and disorders can be clearly identified in the structure of nanocrystalline grains [Figs. 1(a) and 1(b)] due to the introduced residual stress during pulverization process, which should be closely related to the instability of the martensitic transition with varying particle size. Although the visible size of particles under SEM is larger than $0.3\ \mu\text{m}$, the crystallite size is actually in the range about 2–20 nm under high resolution TEM for P4 ($1\text{--}2\ \mu\text{m}$) and P5 ($0.3\text{--}1\ \mu\text{m}$), and the amount of the amorphous structure is 30% and 40%, respectively [Figs. 1(a) and 1(b)]. In this case, grain boundary sliding becomes easier and the introduced residual stress in the grain boundaries of the amorphous structure can be easily spread into lattice and cause atomic defects inside the grains, hence stabilizing the austenite phase with smaller volume and eventually leading to the shift or even disappearance of the martensitic transformation. NPD (neutron powder diffraction) studies²⁴ have revealed that an applied hydrostatic pressure stabilizes the hexagonal structure of Mn–Co–Ge–In through shortening the Mn–Mn interlayer distance and strengthening the covalent bonding between Mn–Mn atoms. Owing to the nonuniform grain size, it is understandable that not all but only a fraction of grains, which contain a higher residual stress and lattice deformation, lose the martensitic transition. The remaining fraction undergoes the martensitic transition in a broadened temperature window (Fig. 3) because of the distribution of residual stress over the various grains.

Figure 4 displays the refined unit cell volume as a function of temperature (V-T curve) for the orthorhombic phase (red dot), hexagonal phase (blue dot), and the calculated average volume \bar{V}

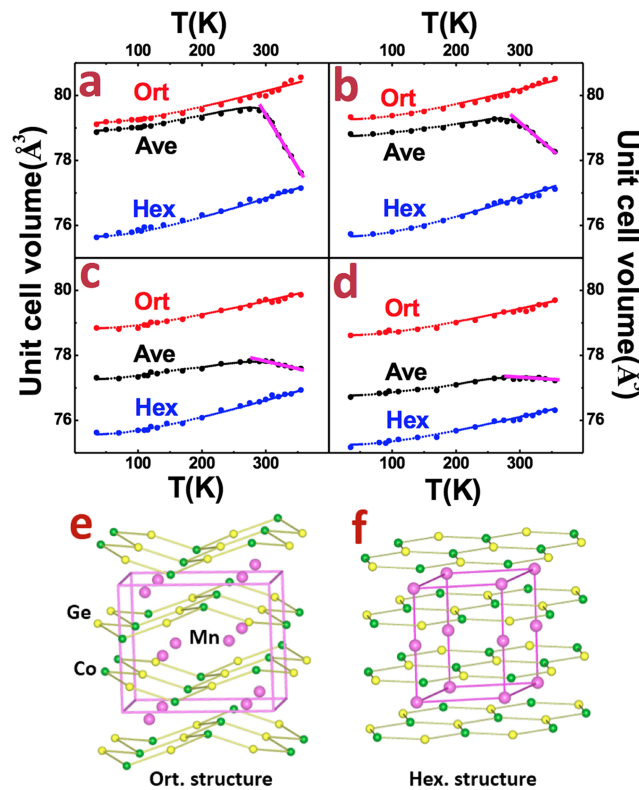


FIG. 4. Refined unit cell volumes of martensitic phase (red dot), austenitic phase (blue dot), and the average (black dot), as a function of temperature for the overall crystalline phases in various particles: (a) P1 ($10\text{--}20\ \mu\text{m}$), (b) P2 ($5\text{--}10\ \mu\text{m}$), (c) P4 ($1\text{--}2\ \mu\text{m}$), and (d) P5 ($0.3\text{--}1\ \mu\text{m}$). The fitting curves based on Grüneisen law are represented by the small dots. Both the PTE and NTE coefficients decline with reducing crystalline size, particularly for the NTE behavior, which is guided by the magenta lines. The sketches of (e) orthorhombic and (f) hexagonal structures vividly show the change of unit cell (magenta lines enclosed) and atomic chain upon martensitic structural transformation.

(black dot) based on the refined phase fraction shown in Fig. 3. To validate the refined cell volume, we also fit the temperature-dependent unit cell volume based on the Grüneisen law,²⁸ where the volume thermal expansion coefficient, α_v , can be approximately described as

$$\alpha_v = (\gamma/k_0)(C_v/V_m), \quad (1)$$

where γ is the macroscopic thermodynamic Grüneisen parameter, k_0 represents the bulk modulus without lattice vibration, V_m is the molar volume, and C_v is the isochoric specific heat per mole. Clearly, α_v is determined by the macroscopic Grüneisen parameter γ and approximately proportional to C_v . It is known that the macroscopic Grüneisen parameter (γ) can be related to the alteration of the vibration frequencies (phonons) within a crystal with changing volume under the quasi-harmonic approximation, i.e., the weighted average of the mode Grüneisen parameters. It can be defined as $\gamma = \frac{\sum_i \gamma_i c_{v,i}}{\sum_i c_{v,i}}$, where $\gamma_i = -d \ln \omega_i / d \ln V$ is the Grüneisen parameter of an individual vibrational mode and $C_{v,i}$ is the partial vibrational mode contributed to the heat capacity. Note that the phonon frequencies, ω_i , are crucially dependent on the unit cell volume, V . Nanocrystalline particles prepared by high-pressure compaction or high energy ball-milling usually suffer stress. The lattice tends to contract with the reduced grain size due to stress.²⁹ This fact indicates that the thermal expansion coefficient, α_v , should be variable for the crystallites with different grain sizes. We measured the isobaric specific heat C_p in a temperature range from 35 K to 355 K for the bulk $\text{MnCoGe}_{0.99}\text{In}_{0.01}$ (Ref. 24) and assumed that $C_p \approx C_v$ and the C_p - T relation would maintain the same as the bulk for the crystallites in different particles. Then the fitting calculation was performed using Eq. (1), where two reliable points of the refined unit cell volumes based on XRD or NPD were used. As shown in Fig. 4, the fitting V - T curves (red and blue line) agree well with the refined points for either orthorhombic or hexagonal phase, confirming that almost all points of the refined unit cell volumes are reliable for the crystallites in different particles.

From the calculated average volume \bar{V} of the overall crystalline phases shown in Fig. 4 (black curve), ignoring the contribution from the amorphous structure, one can notice that PTE appears below a temperature around 290 K and after that turns to be NTE, but both the PTE and NTE coefficients decline and the \bar{V} - T curve becomes flat with the reduced crystallite size (equivalent linear thermal expansion coefficients, $\alpha \sim \Delta L/L/\Delta T$, are summarized in Table I). The reduced PTE and NTE can be mainly ascribed to the instability of the martensitic magnetostructural transformation caused by the introduced residual stress and defects during milling, which round off the transition due to the lattice deformation and softening enforced by stress.^{15,26,27}

Moreover, the bonded samples for $\Delta L/L$ measurements (Fig. 2) experienced a pressure as high as 11.5 kbar before solidification at 170 °C (details can be found in the [supplementary material](#)). The further introduced residual stress during bonding process additionally deforms and softens the lattice, as a result, further broaden the martensitic magnetostructural transformation and significantly extend the temperature window of NTE from the crystallites. Direct $\Delta L/L$ measurements verified the enlarged temperature window of NTE from 60 K to 108 K and its shift to lower temperature for the $\text{MnCoGe}_{0.99}\text{In}_{0.01}$ bulk due to the lattice softening enforced by the introduced residual stress.¹⁵ Detailed magnetic experiments also confirmed the significant broadening of structural/magnetostructural transformation, while the pure magnetic transition remains nearly unaffected in the bonded samples.¹⁵ In this sense, the overall NTE performance from crystallites in the bonded particles can be understood.

TABLE I. The equivalent linear PTE and NTE coefficient α ($\Delta L/L/\Delta T$) in the corresponding temperature window for the overall crystalline phases of typical particles.

Particles	PTE window ΔT (K)	PTE α (K^{-1})	NTE window ΔT (K)	NTE α (K^{-1})
P1 (10–20 μm)	35–280	12.7×10^{-6}	290–355	-134.2×10^{-6}
P2 (5–10 μm)	35–280	10.8×10^{-6}	290–355	-70.5×10^{-6}
P4 (1–2 μm)	35–270	9.2×10^{-6}	275–355	-21.4×10^{-6}
P5 (0.3–1 μm)	35–270	8.5×10^{-6}	275–355	-12.9×10^{-6}

On the other hand, the contribution from the amorphous structure also plays a key role to the overall $\Delta L/L$ behavior (Fig. 2), noting its amount is up to 40% for the smallest particles P5 (0.3–1 μm). One can notice that the low NTE α ($\sim -3.9 \times 10^{-6}/\text{K}$) of the overall P4 (1–2 μm) (Fig. 2) is much smaller than α ($\sim -21.4 \times 10^{-6}/\text{K}$) purely contributed from the nanocrystallites of P4 (1–2 μm) [Fig. 4(c)]. The maximal $\Delta L/L$ in the overall P4 (1–2 μm) (Fig. 2) amounts to ~ 810 ppm, which is also smaller than the equivalent $\Delta L/L$ [~ 970 ppm in an incomplete NTE region 290–355 K, Fig. 4(c)] purely from the free nanocrystallites of P4 (1–2 μm). Moreover, the negative NTE ($\alpha \sim -12.9 \times 10^{-6}/\text{K}$) purely from the free nanocrystallites of P5 (0.3–1 μm) [Fig. 4(d)] turns to be positive PTE ($\alpha \sim +0.68 \times 10^{-6}/\text{K}$) in the overall P5 (0.3–1 μm) (Fig. 2). It has been demonstrated that a self-compensation effect of PTE from the amorphous structure plays an essential role in the realization of ultra-low expansion even if the possible contribution from the epoxy is considered (details can be found in the [supplementary material](#)).

Song *et al.*¹² reported ZTE in nanocrystalline antiperovskite manganese nitrides $\text{Mn}_3\text{Cu}_{0.5}\text{Ge}_{0.5}\text{N}$. The studies indicated that the Mn site occupancy crucially affects thermal expansion because of its dominant role in the coupling between the spin and structure. NTE or ZTE can be reached by adjusting Mn site occupancy with different grain sizes. However, the situation is not the same for the present case, although the Mn atoms also dominate the ferromagnetic properties in Mn–Co–Ge–In, where the driving force for the magnetostructural transition is the crystallographic transition while the magnetic transition occurs cooperatively.^{24,30} The instability of the magnetostructural transition caused by residual stress and defects contributes to the NTE or ZTE behavior. For most of materials with magnetostructural transitions, such as $\text{La}(\text{Fe},\text{Co},\text{Si})_{13}$ (Refs. 31 and 32), Ni–Mn–In (Ref. 33), the stress and magnetic field can both drive the transition. But the case is quite different for the present hexagonal $\text{MM}'\text{X}$ materials, whose magnetostructural transition behaves sensitive to the stress, while insensitive to the magnetic field.²⁴ In other words, it is the lattice rather than spin ordering that dominates the transition. In this sense, the disordered occupation of Mn site caused by defects may not dominantly affect the thermal expansion behavior. Instead, the introduced residual stress and atomic defects play a key role, which not only broadens the magnetostructural transition but also makes a large amount of austenite lose the martensitic structural transition, resulting in a reduced NTE in the nanocrystalline grains. Meanwhile, significant impact of high-energy ball milling creates a large amount of amorphous structures, which turns to show PTE behavior. As a result, self-compensation effect leads to the ultra-low thermal expansion and totally tunable NTE in the bonded Mn–Co–Ge–In particles through quantitatively controlling the crystallinity degree and impacting phase transition.

In summary, we present evidence for the realization of ultra-low thermal expansion in a giant NTE material based on the martensitic magnetostructural transition. This work realizes the ZTE in a single material through self-compensation and conquers the limitation of traditional glass ceramics that require multiple main phases of crystallites. Our studies revealed that the thermal expansion behavior of Mn–Co–Ge–In can be totally adjusted by quantitatively controlling the crystallinity degree and impacting the phase transition from atomic scale. Ultra-low thermal expansion with a thermal expansion coefficient as small as $\alpha \sim +0.68 \times 10^{-6}/\text{K}$ over a temperature range wider than 100 K around room temperature has been achieved in the small particles P5 (0.3–1 μm) through self-compensation, where the amount of the amorphous structure reaches 40% and the ratio of the hexagonal structure that lost the martensitic transformation is 55.2% in the nanocrystallines. We anticipate that it is a universal mechanism that modulating the crystallinity degree and phase transition, independently of the manufacturing process, can precisely tailor the thermal expansion and realize ZTE, particularly from the large class of giant NTE materials based on phase transition, which provides a novel but a very practical avenue to obtain ZTE materials.

See [supplementary material](#) for more detailed information on sample preparation, magnetic measurements, SEM and TEM analyses, and XRD and NPD measurements.

This work was supported by the National Key R&D Program of China (Grant Nos. 2017YFB0702702, 2014CB643700, 2017YFA0303601, and 2016YFB0700903), the National Natural Sciences Foundation of China (Grant Nos. 51531008, 51771223, 51590880, 11474341, and 11674378), and the Strategic Priority Research Program (B) and key program of the CAS.

- ¹ C. L. Rathmann, G. H. Mann, and M. E. Nordberg, *Appl. Opt.* **7**, 819 (1968).
- ² Y. Namba, H. Takehara, and Y. Nagano, *Ann. CIRP* **50**, 239 (2001).
- ³ Z. C. Du, M. R. Zhu, Z. G. Wang, and J. G. Yang, *Compos. Struct.* **152**, 693 (2016).
- ⁴ J. K. Macdowell, *J. Am. Ceram. Soc.* **73**, 2287 (1990).
- ⁵ T. A. Kompan, A. S. Korenev, and A. Y. Lukin, *Int. J. Thermophys.* **29**, 1896 (2008).
- ⁶ T. A. Mary, J. S. O. Evans, T. Vogt, and A. W. Sleight, *Science* **272**, 90 (1996).
- ⁷ X. G. Zheng, H. Kubozono, H. Yamada, K. Kato, Y. Ishiwata, and C. N. Xu, *Nat. Nanotechnol.* **3**, 724 (2008).
- ⁸ J. Chen, K. Nittala, J. S. Forrester, J. L. Jones, J. X. Deng, R. B. Yu, and X. R. Xing, *J. Am. Chem. Soc.* **133**, 11114 (2011).
- ⁹ M. Azuma, W. T. Chen, H. Seki, M. Czapski, S. Olga, K. Oka, M. Mizumaki, T. Watanuki, N. Ishimatsu, N. Kawamura, S. Ishiwata, M. G. Tucker, Y. Shimakawa, and J. P. Attfield, *Nat. Commun.* **2**, 347 (2011).
- ¹⁰ S. Iikubo, K. Kodama, K. Takenaka, H. Takagi, M. Takigawa, and S. Shamoto, *Phys. Rev. Lett.* **101**, 205901 (2008).
- ¹¹ Y. Sun, C. Wang, Q. Z. Huang, Y. F. Guo, L. H. Chu, M. Arai, and K. Yamaura, *Inorg. Chem.* **51**, 7232 (2012).
- ¹² X. Y. Song, Z. H. Sun, Q. Z. Huang, M. Rettenmayr, X. M. Liu, M. Seyring, G. N. Li, G. H. Rao, and F. X. Yin, *Adv. Mater.* **23**, 4690 (2011).
- ¹³ K. Takenaka and H. Takagi, *Appl. Phys. Lett.* **87**, 261902 (2005).
- ¹⁴ R. J. Huang, Y. Y. Liu, W. Fan, J. Tan, F. R. Xiao, L. H. Qian, and L. F. Li, *J. Am. Chem. Soc.* **135**, 11469 (2013).
- ¹⁵ Y. Y. Zhao, F. X. Hu, L. F. Bao, J. Wang, H. Wu, Q. Z. Huang, R. R. Wu, Y. Liu, F. R. Shen, H. Kuang, M. Zhang, W. L. Zuo, X. Q. Zheng, J. R. Sun, and B. G. Shen, *J. Am. Chem. Soc.* **137**, 1746 (2015).
- ¹⁶ K. Takenaka, Y. Okamoto, T. Shinoda, N. Katayama, and Y. Sakai, *Nat. Commun.* **8**, 14102 (2017).
- ¹⁷ J. R. Salvador, F. Gu, T. Hogan, and M. G. Kanatzidis, *Nature* **425**, 702 (2003).
- ¹⁸ K. Takenaka and H. Takagi, *Appl. Phys. Lett.* **94**, 131904 (2009).
- ¹⁹ A. E. Phillips, G. J. Halder, K. W. Chapman, A. L. Goodwin, and C. J. Kepert, *J. Am. Chem. Soc.* **132**, 10 (2010).
- ²⁰ S. Margadonna, K. Prassides, and A. N. Fitch, *J. Am. Chem. Soc.* **126**, 15390 (2004).
- ²¹ S. Niziol, A. Weselucha, W. Bazela, and A. Szytula, *Solid State Commun.* **39**, 1081 (1981).
- ²² E. K. Liu, W. H. Wang, L. Feng, W. Zhu, G. J. Li, J. L. Chen, H. W. Zhang, G. H. Wu, C. B. Jiang, H. B. Xu, and F. D. Boer, *Nat. Commun.* **3**, 873 (2012).
- ²³ L. Caron, N. T. Trung, and E. Bruck, *Phys. Rev. B* **84**, 020414 (2011).
- ²⁴ R. R. Wu, L. F. Bao, F. X. Hu, H. Wu, Q. Z. Huang, J. Wang, X. L. Dong, G. N. Li, J. R. Sun, F. R. Shen, T. Y. Zhao, X. Q. Zheng, L. C. Wang, Y. Liu, W. L. Zuo, Y. Y. Zhao, M. Zhang, X. C. Wang, C. Q. Jin, G. H. Rao, X. F. Han, and B. G. Shen, *Sci. Rep.* **5**, 18027 (2015).
- ²⁵ Y. Liu, F. R. Shen, M. Zhang, L. F. Bao, R. R. Wu, Y. Y. Zhao, F. X. Hu, J. Wang, W. L. Zuo, J. R. Sun, and B. G. Shen, *J. Alloys Compd.* **649**, 1048 (2015).
- ²⁶ J. Schiøtz, F. D. Di Tolla, and K. W. Jacobsen, *Nature* **391**, 561 (1998).
- ²⁷ B. Gilbert, F. Huang, H. Z. Zhang, G. A. Waychunas, and J. F. Banfield, *Science* **305**, 651 (2004).
- ²⁸ G. A. Slack, in *Solid State Physics*, edited by F. Seitz *et al.* (Academic, 1979), pp. 1–71.
- ²⁹ R. Lamber, S. Wetjen, and N. I. Jaeger, *Phys. Rev. B* **51**, 10968 (1995).
- ³⁰ S. Anzai and K. Ozawa, *Phys. Rev. B* **18**, 2173 (1978).
- ³¹ B. G. Shen, J. R. Sun, F. X. Hu, H. W. Zhang, and Z. H. Cheng, *Adv. Mater.* **21**, 4545 (2009).
- ³² L. Manosa, D. Gonzalez-Alonso, A. David, M. Barrio, J. L. Tamarit, I. S. Titov, M. Acet, A. Bhattacharyya, and S. Majumdar, *Nat. Commun.* **2**, 595 (2011).
- ³³ L. Manosa, D. Gonzalez-Alonso, A. Planes, E. Bonnot, M. Barrio, J. L. Tamarit, S. Aksoy, and M. Acet, *Nat. Mater.* **9**, 478 (2010).